THE JOURNAL OF BIOLOGICAL CHEMISTRY VOL. 283, NO. 24, pp. 16702–16710, June 13, 2008

The Stereochemical Course of 4-Hydroxy-2-nonenal Metabolism by Glutathione *S*-Transferases*[S]

Received for publication, March 4, 2008, and in revised form, April 16, 2008 Published, JBC Papers in Press, April 17, 2008, DOI 10.1074/jbc.M801725200

Larissa M. Balogh[‡], Arthur G. Roberts[‡], Laura M. Shireman[‡], Robert J. Greene[§], and William M. Atkins[‡1]

From the [‡]Department of Medicinal Chemistry, University of Washington, Seattle, Washington 98195-7610 and the [§]Department of Pharmacokinetics and Drug Metabolism, Amgen Inc., Seattle, Washington 98119-3105

4-Hydroxy-2-nonenal (HNE) is a toxic aldehyde generated during lipid peroxidation and has been implicated in a variety of pathological states associated with oxidative stress. Glutathione *S*-transferase (GST) A4-4 is recognized as one of the predominant enzymes responsible for the metabolism of HNE. However, substrate and product stereoselectivity remain to be fully explored. The results from a product formation assay indicate that hGSTA4-4 exhibits a modest preference for the biotransformation of *S*-HNE in the presence of both enantiomers. Liquid chromatography mass spectrometry analyses using the racemic and enantioisomeric HNE substrates explicitly demonstrate that hGSTA4-4 conjugates glutathione to both HNE enantiomers in a completely stereoselective manner that is not maintained in the spontaneous reaction. Compared with other hGST isoforms, hGSTA4-4 shows the highest degree of stereoselectivity. NMR experiments in combination with simulated annealing structure determinations enabled the determination of stereochemical configurations for the GSHNE diastereomers and are consistent with an hGSTA4-4-catalyzed nucleophilic attack that produces only the *S*-configuration at the site of conjugation, regardless of substrate chirality. In total these results indicate that hGSTA4-4 exhibits an intriguing combination of low substrate stereoselectivity with strict product stereoselectivity. This behavior allows for the detoxification of both HNE enantiomers while generating only a select set of GSHNE diastereomers with potential stereochemical implications concerning their effects and fates in biological tissues.

Stereochemical configuration is a fundamental aspect of molecular structure, and the functional consequences of dynamic stereochemistry in biology are well established (1–6). Substrate stereoselectivity may occur in enzyme-mediated catalysis by virtue of the innate asymmetry of the active site. Product stereoselectivity may also arise when new chiral centers are introduced during an enzymatic reaction, because enzymes may specifically stabilize only one of the possible transition states for a given reaction. Stereoselective metabolism of both xenobiotic and endogenous molecules is a well recognized phenomenon that reflects this underlying chiral recognition process. To the extent that stereochemically distinct substrates and products have different biological effects, it is essential to define the stereochemical course of enzymatic reactions.

Among the molecules generated endogenously from the degradation of polyunsaturated fatty acids during lipid peroxidation, the unsaturated aldehyde 4-hydroxy-2-nonenal (HNE)[2] has been implicated in a variety of pathological states associated with the deleterious consequences of oxidative stress, including atherosclerosis, diabetes, Alzheimer disease, and Parkinson disease (7–11). HNE has been proposed to exert a number of toxicological effects via its electrophilic α,β– unsaturated carbonyl moiety that can react through additions with nucleophiles such as cysteine, histidine, and lysine residues (12–14). HNE is also involved in modulating a variety of signaling cascades related to proliferation, differentiation, and apoptosis (15, 16). However, stereochemical aspects of many of these processes have not been established.

Glutathione *S*-transferases (GSTs) comprise a family of multifunctional enzymes known to catalyze the conjugation of the tripeptide γ-Glu-Cys-Gly (GSH) with xenobiotic and endogenous electrophiles including HNE (17, 18). The GSTs have several roles, including detoxification of endogenous compounds, drug metabolism, and antioxidant functions. In general, the A class GSTs are known to play a vital role in detoxification of oxidative stress products (19, 20). However, although the GSTA1-1 isoform is regarded as a highly promiscuous enzyme, GSTA4-4 is distinguished by a striking specificity toward HNE and related alkenal substrates (21–24). The discrepancy between specificities in these structurally related GST isoforms has been attributed to a relatively small number of amino acid substitutions and differences in protein dynamics within the constraints of a conserved scaffold.

Conjugation to GSH has been identified as the primary route of HNE detoxification followed by oxidative/reductive modifications and, ultimately, mercapturic acid formation (25–28). Although HNE can spontaneously react with GSH to form a conjugate (GSHNE), GSTs have been found to significantly enhance the rate of this 1,4-addition reaction (see Fig. 1) (14, 29). GSTA4-4 is recognized as one of the predominant iso-

* This work was supported, in whole or in part, by National Institutes of Health Grant GM32165. The costs of publication of this article were defrayed in part by the payment of page charges. This article must therefore be hereby marked "*advertisement*" in accordance with 18 U.S.C. Section 1734 solely to indicate this fact.

[S] The on-line version of this article (available at http://www.jbc.org) contains supplemental Table S1 and supplemental Figs. S1 and S2.

[1] To whom correspondence should be addressed: Box 357610, Dept. of Medicinal Chemistry, University of Washington, Seattle, WA 98195-7610. Tel.: 206-685-0379; Fax: 206-685-3252; E-mail: winky@u.washington.edu.

[2] The abbreviations used are: HNE, 4-hydroxy-2-nonenal; GST, glutathione *S*-transferase; GSHNE, glutathionyl 4-hydroxynonanal; GSDHN, glutathionyl 1,4-dihydroxynonanol; TNBS, 2,4,6-trinitrobenzenesulfonic acid; ROESY, rotating frame Overhauser enhancement spectroscopy; LC/MS, liquid chromatography mass spectrometry; HPLC, high pressure liquid chromatography.

forms responsible for the conjugation of HNE and GSH. Other GSTs in the A, P, and M classes can also contribute to the metabolism of HNE, albeit with significantly reduced activity (19, 23, 24, 30).

Lipid peroxidation generates both enantiomers of HNE; however, monoclonal antibodies that enantioselectively recognized histidine adducts of *R*- or *S*-HNE indicated they had different intracellular localizations in the renal cortex of rats exposed to a carcinogen (31). Furthermore, Hiratsuka *et al.* (32) demonstrated that the *S*-HNE enantiomer irreversibly inactivated rabbit glyceraldehyde-3-phosphate dehydrogenase at a greater rate than *R*-HNE. They also found a stereoselective consumption of substrate by rat GSTA4-4 in the order of *S*-HNE > racemic HNE > *R*-HNE (33), whereas a separate study by Boon *et al.* (28) speculated that product stereoselectivity on behalf of GSTs is one potential explanation for the unequal distribution of GSHNE diastereomers observed in rat liver cytosol. Chirality has also been implicated as an important factor in other enzymes, such as aldehyde-dehydrogenase and aldo-keto reductases, that can also contribute to HNE metabolism and subsequent biotransformations of GSHNE (34–36).

Further work is needed to adequately characterize factors that contribute to the unique roles of the HNE and GSHNE stereoisomers. Previously, the stereoselectivity of human GSTA4-4 (hGSTA4-4) had not been explicitly determined. Two stereochemical processes catalyzed by GSTs have not been completely understood: the relative preference for *R*-HNE *versus S*-HNE, which we refer to as substrate stereoselectivity, and the stereochemical course of GSH addition to the prochiral carbon 3 position, which we refer to as product stereoselectivity. Herein we report that hGSTA4-4 is modestly substrate selective, with a preference for the biotransformation of *S*-HNE in the presence of both enantiomers. Furthermore, for each enantiomeric substrate, hGSTA4-4 conjugates GSH to HNE with complete product stereoselectivity that is not maintained in the spontaneous reaction. NMR analyses were used to characterize the GSHNE diastereomers, and the stereoselectivity of hGSTA4-4 was also compared with other hGST isoforms as well as rationally designed mutants. These results reveal that hGSTA4-4 is unique in its combination of high catalytic efficiency for both HNE enantiomers with a strict product stereoselectivity that yields specific GSHNE diastereomers.

EXPERIMENTAL PROCEDURES

Protein Expression and Purification—Human recombinant GSTA4-4 was expressed as an ubiquitin fusion co-translationally cleaved by a co-expressed ubiquitin-specific protease in *Escherichia coli* and purified via glutathione-agarose affinity chromatography as described previously (21). The subunit concentration was determined by the Edelhoch method (37) using $\epsilon = 15930\ \text{M}^{-1}\ \text{cm}^{-1}$ for denatured hGSTA4-4. Human recombinant GSTA1-1 and P1-1 were expressed and purified in a manner similar to that described previously (38). The human GSTA4-4 F111V/Y217R and GSTA1-1 V111F/R217Y mutants were constructed using overlap extension PCR as described previously (23).

R- and S-HNE—Racemic HNE purchased from Cayman Chemicals (Ann Arbor, MI) was dried at room temperature and reconstituted in a mixture of 98:2 *n*-hexane:isopropanol. The enantiomers were separated by normal phase HPLC on a chiral column (Chiralcel OB; 250 × 4.6 mm, 10-micron particle size; Chiral Technologies, West Chester, PA) eluted with an isocratic mobile phase of *n*-hexane/isopropanol 98.7/1.3 (v/v) at a flow rate of 1 ml/min (32). The *S*- and *R*-HNE enantiomers eluting at 19 and 22 min, respectively, were collected, evaporated in a dark fume hood, and reconstituted in absolute ethyl alcohol (USP grade). The fractions were checked for purity by reinjection, and the concentrations were determined from absorption at 224 nm using $\epsilon = 13750\ \text{M}^{-1}\ \text{cm}^{-1}$ for HNE in water. Stock solutions were stored in ethanol at −80 °C.

Stereoselectivity Analysis—The diastereomeric GSHNE conjugates were prepared by spontaneous or enzymatic reactions of GSH with HNE. GSH (500 μM) was preincubated with either hGSTA4-4 (3 μM), hGSTA1-1 (33 μM), hGSTP1-1 (33 μM), or buffer alone (100 mM $NaPO_4$, pH 6.6) at 30 °C followed by reaction with racemic or *R*- or *S*-HNE (250 μM) for 3 min. Diastereomer formation was analyzed by LC/MS as described below.

Enzyme Kinetics—The metabolism of HNE (0–150 μM) by hGSTA4-4 (600 pM) in the presence of 1 mM GSH and 100 mM sodium phosphate buffer, pH 6.6, was monitored by product formation. GSH was preincubated with or without hGSTA4-4 in a plate format at 30 °C. Stock HNE solutions (0.5–150 mM in ethanol) were diluted into the appropriate amount of buffer, and reactions were initiated by the addition of HNE to the hGSTA4-4-GSH solutions (1% final ethanol v/v) to produce the final concentrations listed above. After 50 s, 200 μl of each reaction was quenched with 50 μl of a cold acetic acid:methanol (20:80 v/v) solution containing 5 μM caffeine as an internal standard. GSHNE diastereomer formation was analyzed by LC/MS (*m/z* 464) as described below. The data points represent the averages of duplicate assays and have been corrected for the corresponding spontaneous reaction. The standard curves were generated from known amounts of purified GSHNE diluted to the same extent with quench solution. Kinetic constants were determined by nonlinear regression using GraphPad Prism version 4.00 for Windows (GraphPad Software, San Diego, CA).

Preparation of the GSHNE Diastereomers—GSHNE was synthesized by incubating HNE with excess GSH. The resulting diastereomers were separated by reverse phase HPLC on a C18 column (Econosphere C18; 250 × 10 mm; Alltech, Deerfield, IL) eluted with an isocratic mobile phase of 16% acetonitrile and 0.1% formic acid in water at a flow rate of 5 ml/min. The fractions were collected and analyzed by LC/MS as described below, and the appropriate fractions were pooled. This process was repeated until sufficient amounts of the diastereomers were obtained for NMR analysis or use in a standard curve. A Rotavap was used to remove the organic in the mobile phase, and the remaining solution was frozen and lyophilized.

Reduction of GSHNE by $NaBH_4$—The hGSTA4-4 enzyme was used in separate incubations with GSH and *R*- or *S*-HNE to generate the GSHNE peak I and II diastereomers, respectively. GSHNE was maintained in linear form by reducing the aldehyde to produce GS-1,4-dihydroxynonanol (GSDHN). To accomplish this a 0.2 M NaOH solution containing a 20-fold molar excess of $NaBH_4$ was added to the diastereomers (1:1 v/v)

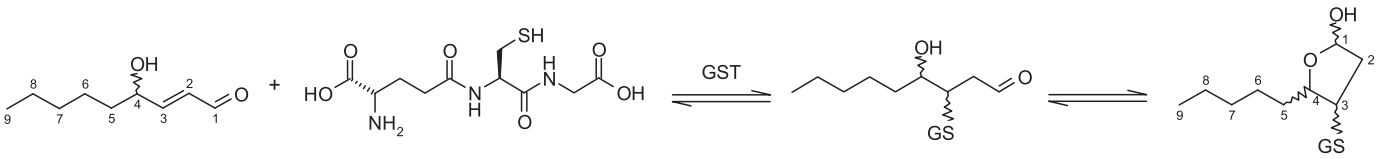

FIGURE 1. **Reaction of HNE with GSH.** 1,4-Addition reaction followed by an intramolecular cyclization is shown.

(39). After 2 h the reaction was quenched by slowly adding 1 M HCl on ice to achieve a pH of 7.0. The solution was concentrated, and the reduced form of GSHNE was purified by reverse phase HPLC as described above. Fractions were then analyzed by LC/MS (*m/z* 466) similar to that described below and characterized by NMR.

Quantification of GSHNE—The GSHNE conjugates were prepared and purified as described above, and stock concentrations were then determined using a 2,4,6-trinitrobenzenesulfonic acid (TNBS) assay (40). The absorption of the TNBS derivative was monitored at 335 nm on a Cary 3E UV-Visible spectrophotometer (Varian, Cary, NC) equipped with Cary WinUV software. The concentration of primary amines, and hence the concentration of GSHNE, was determined via linear regression of a standard curve generated from a 0.025% TNBS solution and 50–250 μM GSH.

Liquid Chromatography Mass Spectrometry Analysis—LC/MS analyses were conducted on a Waters Alliance 2690 HPLC system interfaced to a Waters Micromass Platform LCZ quadrupole mass spectrometer (Waters Corp., Milford, MA). The GSHNE diastereomers were separated by reverse phase HPLC using a C18 column (Alltima C18; 150 × 2.1 mm; Alltech) equipped with a guard column (4 × 3 mm) and eluted with an isocratic mobile phase of 16% acetonitrile and 0.1% formic acid in water at a flow rate of 0.3 ml/min (41). The desolvation temperature was set to 350 °C, and the cone voltage was maintained at 20 kV. Mass spectral analyses on the kinetic incubations were carried out on 10-μl injections with selected ion monitoring for both the internal standard caffeine (*m/z* 195.19) and the diastereomeric GSHNE conjugates (*m/z* 464), utilizing electrospray ionization in the positive ion mode. All of the data were analyzed using Micromass Masslynx V4.0 software.

NMR Experiments—Samples containing GSH, GSHNE, or GSDHN were prepared in 70% D_2O, and both one-dimensional NMR spectra and two-dimensional ^1H-^1H correlation spectroscopy and rotating frame Overhauser enhancement spectroscopy (ROESY) ^1H NMR spectra were acquired at 25 °C on a Varian Unity Inova 500 MHz NMR spectrometer, equipped with a Varian triple resonance/pulse field gradient probe (Varian, Inc., Palo Alto, CA). Water suppression was obtained by gradient tailored excitation, and data processing was conducted using MestReC software version 4.9.9.6 (A Coruña, Spain). Three-dimensional conformations of the GSHNE diastereomers were modeled using the Crystallography and NMR System (CNS) software (42). Energy minimized structures were calculated by performing simulated annealing structure determinations on the potential stereochemical configurations for GSHNE with and without the distance restraint estimates obtained from the analysis of two-dimensional ROESY NMR data, using parameters selected from the all-hydrogen (PARALLHDG) geometric energy function parameter set. Relative energies calculated for each combination were used to select the best fit stereochemical configurations.

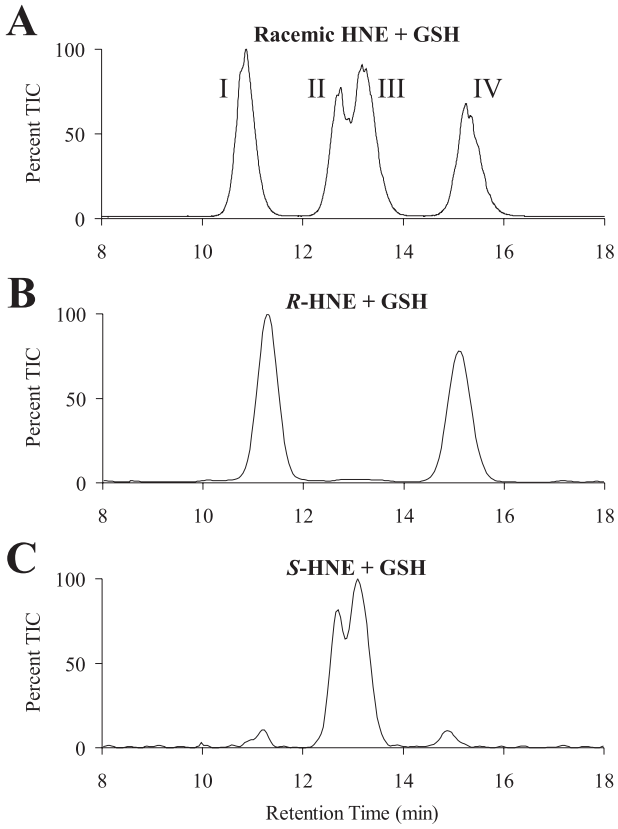

FIGURE 2. **Spontaneous formation of the diastereomeric GSHNE conjugates.** The GSHNE diastereomers were prepared by incubating GSH with racemic (*A*), *R*-HNE (*B*), or *S*-HNE (*C*) and analyzed by LC/MS (electrospray positive ion mode, selected ion monitoring 464). The appearance of small amounts of *peaks I* and *IV* in the LC/MS chromatogram for the *S*-HNE reaction is a result of corresponding *R*-HNE impurities present in our *S*-HNE fraction.

RESULTS

Spontaneous Formation of the Diastereomeric GSHNE Conjugates—HNE spontaneously reacts with GSH to form an adduct with a new chiral center generated at the site of conjugation (Fig. 1). Equilibrium favors the cyclic hemiacetal structure produced from the intramolecular reaction of the 4-hydroxyl group with the aldehyde, which creates an additional chiral center in the molecule (14). Similar to results previously obtained by Ji *et al.* (41), the spontaneous reaction of racemic HNE with GSH produced a LC/MS spectrum with four major diastereomeric peaks (Fig. 2*A*). Taking into account the chiral centers inherent in GSH, there are eight potential GSHNE diastereomers in total, and it is possible that each of the four peaks constitute a pair of unresolved diastereomers. To obtain a partial assignment of configuration and correlate the absolute

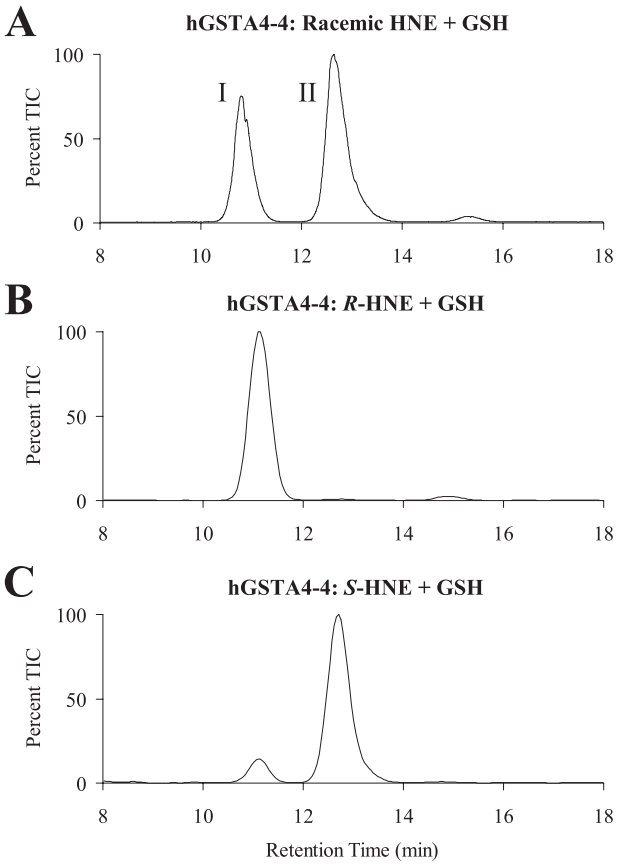

FIGURE 3. **GSTA4-4-catalyzed formation of the diastereomeric GSHNE conjugates.** The GSHNE diastereomers were prepared by incubating hGSTA4-4 and GSH with racemic (*A*), *R*-HNE (*B*), or *S*-HNE (*C*) and analyzed by LC/MS (electrospray positive ion mode, selected ion monitoring 464). The appearance of a small amount of peak I in the LC/MS chromatogram for the *S*-HNE reaction is a result of corresponding *R*-HNE impurities present in our *S*-HNE fraction.

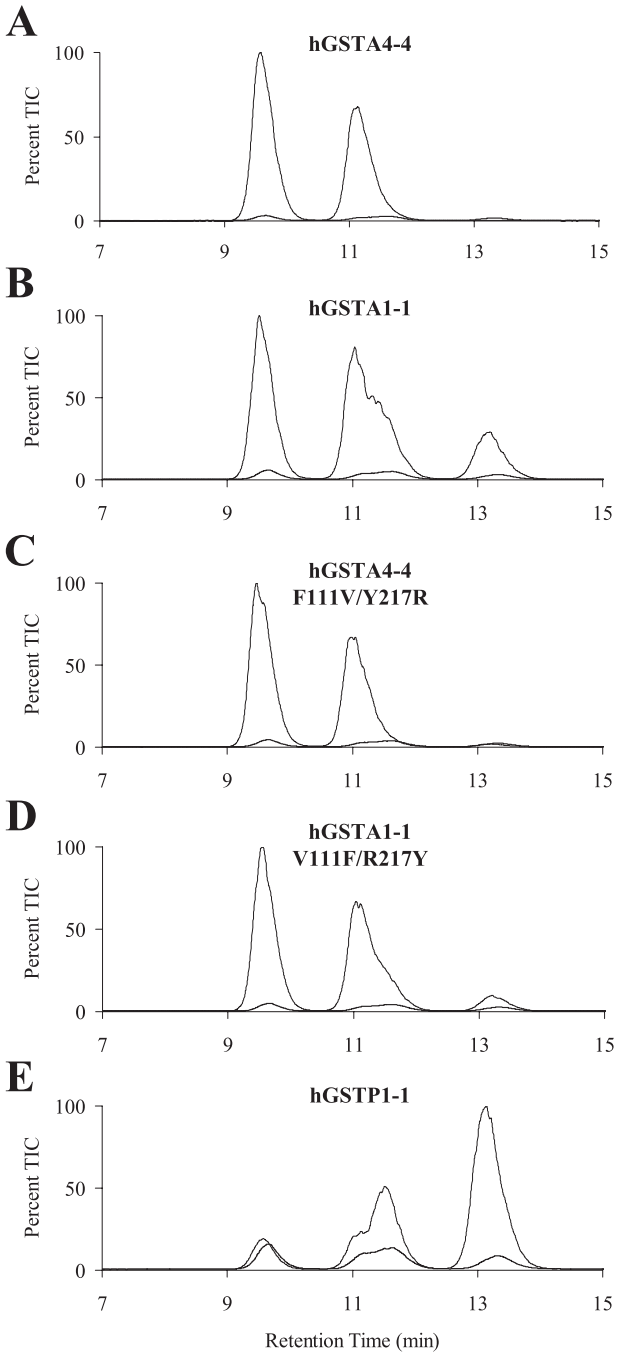

FIGURE 4. **Comparison of product stereoselectivity between hGST isoforms.** The GSHNE diastereomers were prepared by incubating GSH and hGSTA4-4 (*A*), hGSTA1-1 (*B*), hGSTA4-4 F111V/Y217R (*C*), hGSTA1-1 V111F/R217Y (*D*), and hGSTP1-1 (*E*) with racemic HNE and analyzed by LC/MS (electrospray positive ion mode, selected ion monitoring 464). The maximum contribution possible from the spontaneous reaction is also shown in each chromatogram for comparison.

stereochemistry originating from the hydroxyl group with retention time, the enantioisomeric HNE substrates were also used in separate incubations with GSH. The diastereomers derived from the spontaneous reaction for *R*-HNE co-elute with two of the four peaks seen in the racemic reaction (Fig. 2*A*, *peaks I* and *IV*), whereas the diastereomers derived from *S*-HNE co-elute with the remaining two peaks (Fig. 2*A*, *peaks II* and *III*). These results (Fig. 2, *B* and *C*) indicate that the differences in retention time for peaks I and IV, and likewise for peaks II and III, are a result of opposite configurations at the site of GSH conjugation and not at the carbon bearing the hydroxyl group.

Product Stereoselectivity of hGSTA4-4—To determine whether hGSTA4-4 displays stereoselectivity in the production of GSHNE, LC/MS analyses of incubations of GSH with the racemic and enantioisomeric HNE substrates were conducted in the absence and presence of hGSTA4-4. As reported above, the spontaneous reaction produced a LC/MS spectrum with four major peaks. However, as shown in Fig. 3*A*, when hGSTA4-4 catalyzed this reaction, only two of the peaks (peaks I and II) were observed, indicating that hGSTA4-4 conjugates GSH to HNE in a stereoselective manner that is not maintained in the spontaneous reaction. Furthermore, these results, as well as the outcome obtained with the individual HNE enantiomers (Fig. 3, *B* and *C*), establish that the GSHNE peak I and II diastereomers are stereoselectively derived from the hGSTA4-4 catalyzed conjugation of GSH with *R*- and *S*-HNE, respectively. Although all four peaks are generated in relatively small and roughly equal amounts by the spontaneous reaction, the GSHNE peak III and IV diastereomers are exclusively derived from the spontaneous reaction.

Product Stereoselectivity of Other hGST Isoforms—Similar LC/MS experiments were conducted to compare the stereos-

electivity of hGSTA4-4 with other hGST isoforms. Shown in Fig. 4*B* are results acquired with racemic HNE using A1-1, which indicate that it is less product stereoselective than A4-4. These two isoforms share 52% sequence identity and are known to share similar overall topologies, dimer interactions, and conserved GSH-binding sites (22). Despite their numerous similarities, these isoforms show a high degree of variability in their substrate specificities, including a dramatic preference by GSTA4-4 for lipid peroxidation products (22–24).

Unique structural attributes in the C-terminal region are already known to be important for the high catalytic efficiency of A4-4 with HNE (22, 43) and, speculatively, can be implicated in stereoselectivity as well. To explore this issue, the hGSTA4-4 F111V/Y217R and hGSTA1-1 V111F/R217Y mutants previously generated in our lab were also inspected for stereoselectivity. The hGSTA4-4 enzyme contains an edge-to-face aromatic-aromatic interaction between Phe-111 and Tyr-217 that is absent in hGSTA1-1. The interaction between these two residues contributes to a closer association between the α4-α5 helix-turn-helix and C-terminal regions of hGSTA4-4. The mutants eliminate and incorporate this interaction into hGSTA4-4 and hGSTA1-1, respectively, and were recently shown to yield substrate specificity and stability toward denaturants between that of the two wild-type proteins (23). In line with this trend, the LC/MS results show that the mutants are more stereoselective than A1-1 but still less stereoselective than A4-4 (Fig. 4, *C* and *D*). The chromatographic resolution of GSHNE peaks I and IV provides a facile opportunity to quantitatively compare the stereoselectivity of related hGST isofoms. Using the peak IV/I ratio as an indication of the stereoselectivity of GSH attack at carbon 3 of *R*-HNE, hGSTA4-4 has the highest degree of stereoselectivity (IV/I = 0) followed next by hGSTA4-4 F111V/Y217R (IV/I = 0.02), hGSTA1-1 V111F/R217Y (IV/I = 0.12), and lastly hGSTA1-1 (IV/I = 0.39). Also reported in Fig. 4*E* are results from hGSTP1-1 catalysis, where not only was the enzyme less stereoselective, but it also catalyzed the formation of the diastereomers with the opposite configuration at the site of conjugation compared with the A class GSTs tested.

NMR Characterization and Simulated Annealing to Assign Absolute Stereochemistry—GSHNE contains three chiral centers in the cyclic hemiacetal portion of the structure, and the resulting complicated diastereotopic splittings as well as contributions from multiple conformers make the ^{1}H NMR spectrum complex to directly analyze. To facilitate identification, some of the diastereomers were subjected to separate characterizations by NMR. We were able to isolate three of the GSHNE diastereomers (peaks I, II, and IV) as well as the reduced forms (GSDHN) of peaks I and II. We observed signals near 5.5 ppm, which were assigned to the 1-H of GSHNE and are consistent with the cyclic hemiacetal form of HNE adducts (44, 45). The NMR spectrum of GSDHN had better resolution and contained most of the analogous protons from GSHNE with the notable exception of the aforementioned 1-H resonance. The nonequivalence of Cys H$^{\beta1}$ and H$^{\beta2}$ as well as a contribution from only one stereochemical configuration at 3-H were evident in the GSDHN spectrum (Fig. 5). Assignments of all the proton signals were ultimately made by analyzing the one-dimensional ^{1}H NMR spectrum of samples containing GSH, GSHNE, or GSDHN in addition to the correlation spectroscopy and ROESY NMR spectra of GSHNE. A correlation was observed between the 3-H of the tetrahydrofuran moiety and the Cys H$^{\beta}$ protons in all GSHNE samples, indicative of GSH conjugation occurring via a 1,4-addition reaction. Compared with the peak I diastereomer, the chemical shifts of two stereochemically relevant protons (3-H and 4-H) as well as the Cys H$^{\beta}$ protons were shifted downfield in the corresponding spectra of GSHNE peaks II and IV (supplemental Table S1). Analysis of the cross-peaks from the ROESY spectra revealed two through-space correlations that are present in the GSHNE peak I diastereomer (Fig. 6) but weak or absent in the peak II and peak IV diastereomers. Furthermore, the GSHNE peak II and peak IV ROESY spectra contained a correlation between one conformation of the 3-H and 4-H protons (supplemental Fig. S1) that was absent in the peak I diastereomer, suggesting that the peak II and IV diastereomers are in the *cis*-conformation with respect to 3-H and 4-H of the cyclic hemiacetal structure. The *cis*-conformation in combination with the carbon 4 configuration determined above (Fig. 2, *B* and *C*) indicates that the peak II and IV diastereomers correspond to 3*S*,4*S*-GSHNE and 3*R*,4*R*-GSHNE, respectively.

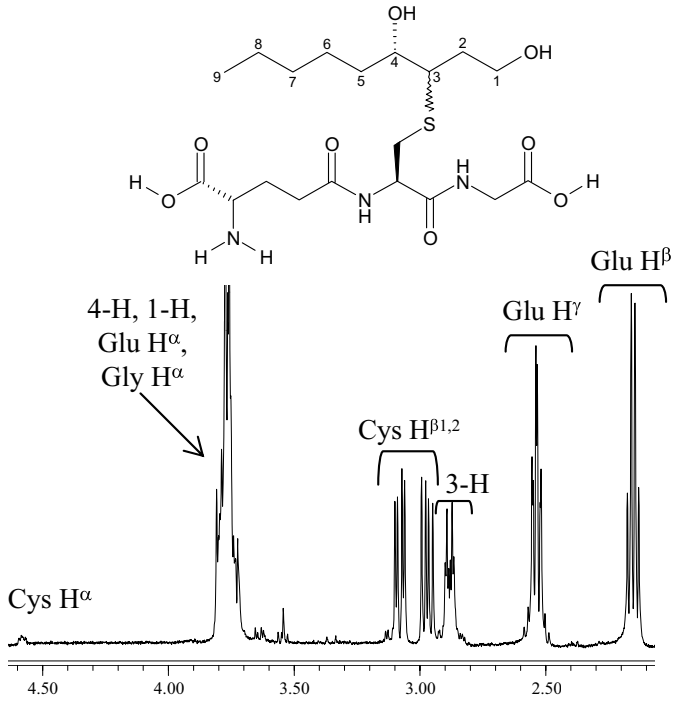

FIGURE 5. **GSDHN diastereomer derived from GSHNE peak II.** 500-MHz one-dimensional ^{1}H NMR spectrum acquired in 70% D_2O and proton assignments for the 2.1–4.6 ppm region were used to help identify the corresponding protons in the spectrum of GSHNE.

The results from the ROESY NMR experiments were also subsequently used to model three-dimensional conformations of the different GSHNE diastereomers derived from *R*-HNE. CNS is a widely used software system capable of incorporating nuclear Overhauser effect-derived distance restraints into a three-dimensional macromolecular structure determination (42). Energy-minimized structures were calculated by performing simulated annealing structure

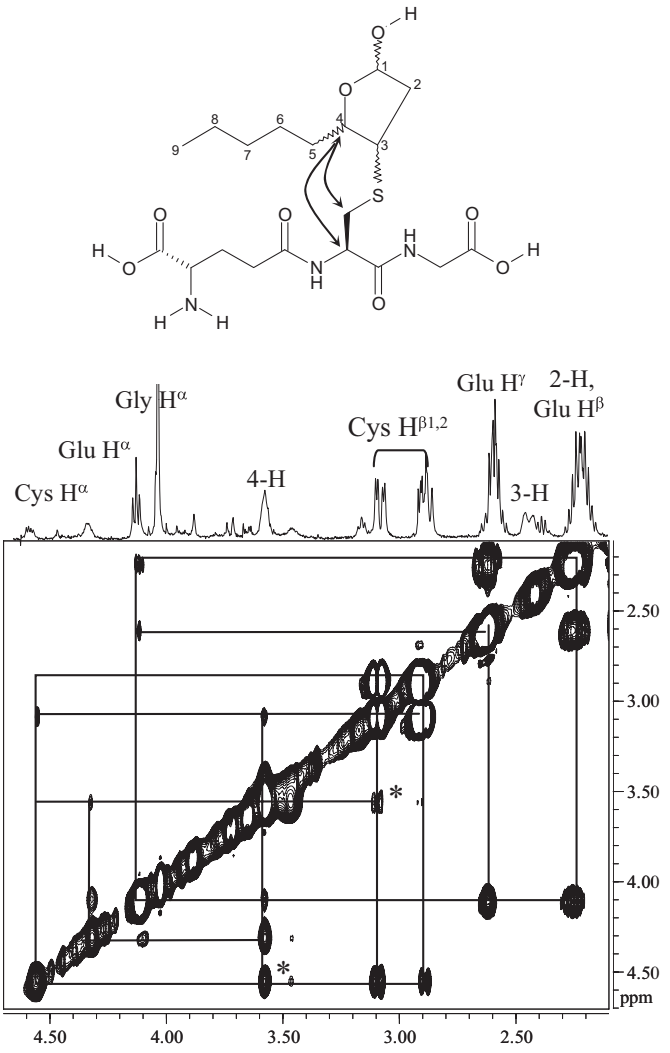

FIGURE 6. **GSHNE peak I.** 500 MHz two-dimensional ROESY ^{1}H NMR spectrum acquired in 70% D_2O and proton assignments for the 2.1–4.6 ppm region are shown. The cross-peaks (through-space correlations) are denoted by *black lines*. The cross-peaks marked with *asterisks* are weak or absent in the analogous spectra of GSHNE peaks II and IV and correspond to an interaction between the 4-H and Cys protons as indicated in the structure.

determinations with and without each set of distance restraint estimates obtained from the ROESY NMR data in combination with each of the potential stereochemical configurations for GSHNE derived from *R*-HNE. The relative energies calculated for each combination identified the best fit stereochemical configuration for the GSHNE peak I and IV diastereomers as 3*S*,4*R*-GSHNE and 3*R*,4*R*-GSHNE, respectively. Because of limited quantities of peak III, the analogous simulated annealing calculation could not be conducted to compare the relative energies of the GSHNE diastereomers derived from *S*-HNE. However, as described above, the chemical shifts and cross-peaks in the one- and two-dimensional NMR spectra for peak II, particularly the 3-H to 4-H ROE correlation, are consistent with that of peak IV, which suggests that it also is in the *cis*-conformation with respect to 3-H and 4-H of the cyclic hemiacetal structure and therefore implies the *trans*-conformation for the GSHNE peak III diastereomer, which corresponds to 3*R*,4*S*-GSHNE.

TABLE 1
Stereochemical configurations of the GSHNE diastereomers

Structure	Peak	Stereochemistry
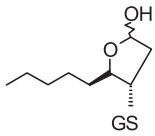	I	3*S*,4*R*-GSHNE
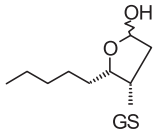	II	3*S*,4*S*-GSHNE
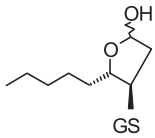	III	3*R*,4*S*-GSHNE
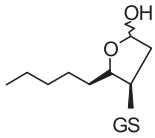	IV	3*R*,4*R*-GSHNE

Table 1 summarizes the stereochemical configurations for the GSHNE diastereomers.

Kinetic Characterization of the hGSTA4-4-mediated GSH Conjugation of HNE—Human GSTA4-4 was incubated with varying concentrations of racemic HNE, and the kinetic parameters for total product formation (K_m = 34 μM, k_{cat} = 100 s^{-1}) determined by nonlinear regression are consistent with previously reported constants (24) for racemic HNE and A4-4 (supplemental Fig. S2*A*). In contrast to the widely used spectral assay that monitors depletion of the substrate double bond (29), the kinetic study used to generate the data reported in this section was conducted using an LC/MS product formation assay that allowed for the concurrent detection of each GSHNE diastereomer. This product formation assay was therefore implemented to examine the simultaneous metabolism of the individual substrate enantiomers by hGSTA4-4 in the presence of racemic HNE as it presumably exists *in vivo*. Slight changes to 39 and 28 μM were observed in the apparent K_m constants for *S*- and *R*-HNE, respectively (supplemental Fig. S2*B*). The relative k_{cat} for *S*-HNE was 2-fold higher than that for *R*-HNE. Variations in the apparent K_m and the relative contributions to k_{cat} ultimately resulted in a 1.5-fold greater catalytic efficiency for *S*-HNE in the hGSTA4-4-mediated conjugation.

DISCUSSION

A variety of studies have utilized different models or species, and a complex picture has emerged with respect to the potential biological ramifications of HNE chirality. Although both HNE enantiomers likely contribute to reported effects, different targets and routes of detoxification could be elicited as a consequence of stereoselectivity. Previous work on hGSTA4-4 has focused on racemic HNE, and hence stereoselectivity as

well as any of its subsequent consequences remain to be fully explored. The studies detailed herein aim to examine substrate and product stereoselectivity and also to identify the different GSHNE diastereomers through LC/MS and NMR characterizations. Comparisons among hGST isoforms were also performed and provide structural implications concerning stereoselectivity within the topography of the active site for these GST enzymes.

In mammals, the cytosolic GSTs are functional dimers that contain one active site per monomer (17). Each active site consists of GSH- and substrate-binding sites, the G-site and H-site, respectively. None of the existing crystal structures capture HNE bound to the H-site, but on the basis of the structure for apo hGSTA4-4 and hGSTA4-4 in complex with the inhibitor S-(2-iodobenzyl)-GSH, Bruns *et al.* (22) predicted that either enantiomer of HNE could fit into the binding pocket. Their model also anticipates that the nucleophilic attack by the GSH sulfur will produce the *S*-configuration at the site of conjugation in the resulting GSHNE diastereomer. Our results experimentally confirm both of these proposals.

The results of the present study explicitly demonstrate that hGSTA4-4 conjugates GSH to HNE in a stereoselective manner that is not maintained in the spontaneous reaction. The GSHNE peak I and peak II diastereomers are derived from the hGSTA4-4 catalyzed metabolism of *R*- and *S*-HNE, respectively, whereas the GSHNE peak III and peak IV diastereomers arise solely from the spontaneous reaction, which produces small amounts of all four peaks. Furthermore, NMR experiments in combination with simulated annealing structure determinations are consistent with an hGSTA4-4-catalyzed nucleophilic attack that produces only the *S*-configuration at the site of conjugation, regardless of substrate chirality.

Although GSTA4-4 and GSTA1-1 have similar overall topologies, dimer interactions, and conserved GSH-binding sites, the specificity of A4-4 contrasts sharply with that of A1-1. Whereas A4-4 has much higher activity toward alkenal substrates, A1-1 is highly promiscuous with catalytic activity toward substrates with a large degree of structural variability (19, 23, 24). The hGSTA4-4 crystal structure-based model as well as mutagenesis indicates that the presence of Tyr-212 in the α9 C-terminal helix is critical for binding and activating HNE (22). Other well characterized structural differences also reside in the C-terminal helix of these enzymes. Apo GSTA1-1 contains a highly disordered C terminus that converts to a more ordered helix upon ligand binding (46). In contrast, the C terminus of GSTA4-4 exists as a well defined α9 helix that provides pre-existing ligand complementarity (22). LC/MS experiments conducted herein raised the possibility that C-terminal dynamics may also contribute to product stereoselectivity. An interaction between Phe-111 and Tyr-217 contributes to a closer association among the α4-α5 helix-turn-helix and C-terminal regions of hGSTA4-4, whereas this area has a high degree of conformational heterogeneity in A1-1 (23). The incorporation of this interaction into hGSTA1-1 resulted in a mutant with a less dynamic C terminus and increased selectivity for HNE. In line with this previous observation, the results reported in this paper indicate that the hGSTA4-4 F111V/Y217R and hGSTA1-1 V111F/R217Y mutants display stereoselectivity intermediate between wild-type A4-4 and A1-1, suggesting that conformational heterogeneity is inversely correlated with product stereoselectivity in these isoforms. This is particularly interesting in light of the substrate stereopromiscuity discussed below.

A marked decrease in stereoselectivity was also observed for hGSTP1-1, which catalyzes the formation of diastereomers with the opposite configuration at the site of conjugation compared with the A class GSTs tested. Comparisons of GSH in the G-site of the hGSTA4-4, A1-1, and P1-1 crystal structures indicate that GSH is always oriented in the same direction. However, the trend in diastereomer formation observed with P1-1 invites speculation regarding the orientation of HNE in the H-site. The physiological significance of this result is unclear given that hGSTP1-1 is reported to have a 400-fold lower catalytic efficiency with HNE as well as a different tissue expression pattern (30). Nevertheless, because P1-1 lacks the aforementioned C-terminal helix (47, 48), these results lend additional support to a role for this region in the specific stereoselectivity observed for A4-4.

The stereochemistry at the site of conjugation could have significant impact on GSHNE bioactivity, transport, and further metabolism. For example, one intriguing study by Ramana *et al.* (49) indicated that the GSDHN metabolite, generated by the aldose reductase-catalyzed aldehyde reduction of GSHNE, is a novel mediator of the cell signaling associated with HNE. Stereochemical configuration presumably would influence the bioactivity of GSDHN, which was reported to stimulate protein kinase C, NF-κB, and AP-1. At least one study already points to an important role for stereochemistry in the reduction of GSHNE to GSDHN. Incubations of GSHNE with rat liver cytosolic fractions resulted in GSDHN originating largely from the GSHNE diastereomer(s) derived only from *R*-HNE, thereby implicating a member of the aldo-keto reductase family (35). Furthermore, a study conducted by Ji *et al.* (41) reported an unequal distribution of the GSHNE diastereomers in the apical compartment of multidrug resistance protein 2 Madin-Darby canine kidney II cells. Although distributions such as these could simply originate from stereoselective GSHNE production, the potential also exists for a stereoselective contribution by a transporter such as multidrug resistance protein 2 or a Ral-binding protein (RLIP76), which has been reported to be largely responsible for the primary, active transport process that exports GSHNE or subsequent metabolites from the cell (50). Collectively, these observations suggest that the GSHNE diastereomers would have different effects and fates in biological tissues.

With respect to the metabolism of the primary substrate, stereoselectivity for *R- versus S*-HNE could also play an important role in the efficient detoxification of these reactive electrophiles. To examine the simultaneous metabolism of the individual HNE enantiomers from within the biologically relevant mixture, the catalytic studies reported herein used a LC/MS product formation assay sensitive to GSHNE stereochemistry. The results demonstrated that hGSTA4-4 shows a modest but significant preference for the biotransformation of *S*-HNE. Variations in the apparent K_m and the relative contributions to

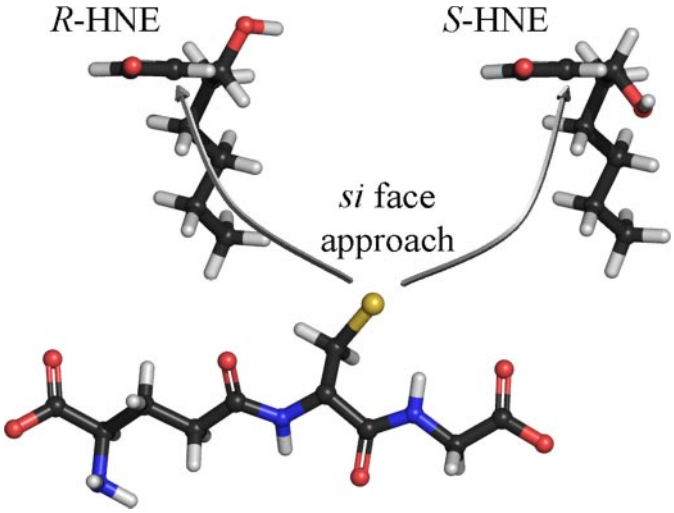

FIGURE 7. **Stereoselective GSH conjugation to HNE catalyzed by hGSTA4-4.** Both enantiomers of HNE as viewed directly along the 2,3-double bond axis, showing the relative orientation of the GSH thiolate and the 2,3-double bond of HNE within the context of the hGSTA4-4 active site. To achieve the observed product stereoselectivity, the nucleophilic attack occurs from the *si* face of the double bond for both HNE enantiomers resulting in the *S*-configuration at the site of conjugation. This orientation places the hydroxyl group of each enantiomer on opposite sides of the active site. Thus, the hydroxyl group is either not exploited for binding, or else there are interactions that are energetically comparable, such as interactions with a symmetrically located residue or enantiospecific interactions with different residues. The structures are color-coded according to atoms. *Red*, oxygen; *blue*, nitrogen; *yellow*, sulfur; *gray*, carbon; *white*, hydrogen.

k_{cat} ultimately resulted in a 1.5-fold greater catalytic efficiency for *S*-HNE.

Despite the slight preference for *S*-HNE as a substrate, hGSTA4-4 was still found to exhibit a remarkably high apparent activity for either enantiomer relative to that reported for other hGST isoforms (19, 30). These results stress that although hGSTA4-4 is a minor GST isoform, its presence can play a crucial role in the detoxification of both HNE enantiomers. Our results also reveal a striking product stereoselectivity intrinsic to hGSTA4-4. Although the high catalytic efficiency for racemic HNE was previously well established, the results herein suggest that the prominent feature of hGSTA4-4 may extend to include its ability to maintain high substrate specificity in conjunction with low substrate stereoselectivity yet strict product stereoselectivity. This dichotomy between substrate stereopromiscuity and product stereoselectivity has biological and enzymological implications. Biologically, this combination allows for the acceptance of both enantiomers as substrates, which provides protection from the harmful consequences of oxidative stress products that can be formed as a racemate, while producing only a select set of GSHNE diastereomers. As noted above, the stereochemical aspects of GSHNE in toxicity, signal transduction, and transport remain to be determined. Further research into the potential stereochemical implications concerning these diastereomers will help to elucidate the significance of chirality regarding the subsequent metabolism, bioactivity, and transport of GSHNE and related metabolites. Enzymologically, it is an intriguing combination of promiscuity and specificity. To achieve the product stereoselectivity that is observed, the relative orientation of GSH and the 2,3-double bond of HNE must be the same for both *R*-HNE and *S*-HNE (Fig. 7). In turn, this places the hydroxyl group of each of the substrates on opposite sides of the active site. Thus, the hydroxyl group is either not exploited for binding, or else there are interactions that are energetically comparable, such as interactions with a symmetrically located residue or enantiospecific interactions with different residues. Further studies are required to understand these aspects of HNE metabolism.

Acknowledgments—We gratefully acknowledge Prof. Philip Board (Australian National University) for providing the construct to express hGSTA4-4, Kei-cheuk Ng for help with protein expression and purification, and Abhinav Nath for assistance with the CNS software.

REFERENCES

1. Burke, D., and Henderson, D. J. (2002) *Br. J. Anaesth.* **88,** 563–576
2. Eichelbaum, M., and Gross, A.S. (1996) in *Advances in Drug Research*, Vol. 28, pp. 1–64, Academic Press, London
3. Jamali, F., Mehvar, R., and Pasutto, F. M. (1989) *J. Pharm. Sci.* **78,** 695–715
4. Smith, D. F. (1989) *Pharmacol. Toxicol.* **65,** 321–331
5. Testa, B. (1986) *Trends Pharmacol. Sci.* **7,** 60–64
6. Walle, T., and Walle, U. K. (1986) *Trends Pharmacol. Sci.* **7,** 155–158
7. Hu, W., Feng, Z., Eveleigh, J., Iyer, G., Pan, J., Amin, S., Chung, F. L., and Tang, M. S. (2002) *Carcinogenesis* **23,** 1781–1789
8. Siegel, S. J., Bieschke, J., Powers, E. T., and Kelly, J. W. (2007) *Biochemistry* **46,** 1503–1510
9. Uchida, K. (2003) *Prog. Lipid Res.* **42,** 318–343
10. Volkel, W., Sicilia, T., Pahler, A., Gsell, W., Tatschner, T., Jellinger, K., Leblhuber, F., Riederer, P., Lutz, W. K., and Gotz, M. E. (2006) *Neurochem. Int.* **48,** 679–686
11. Zarkovic, K. (2003) *Mol. Aspects Med.* **24,** 293–303
12. Carini, M., Aldini, G., and Facino, R. M. (2004) *Mass Spectrom. Rev.* **23,** 281–305
13. Schaur, R. J. (2003) *Mol. Aspects Med.* **24,** 149–159
14. Esterbauer, H., Schaur, R. J., and Zollner, H. (1991) *Free Radic. Biol. Med.* **11,** 81–128
15. West, J. D., and Marnett, L. J. (2005) *Chem. Res. Toxicol.* **18,** 1642–1653
16. Yang, Y., Sharma, R., Sharma, A., Awasthi, S., and Awasthi, Y. C. (2003) *Acta Biochim. Pol.* **50,** 319–336
17. Armstrong, R. N. (1997) *Chem. Res. Toxicol.* **10,** 2–18
18. Hayes, J. D., Flanagan, J. U., and Jowsey, I. R. (2005) *Annu. Rev. Pharmacol. Toxicol.* **45,** 51–88
19. Zhao, T., Singhal, S. S., Piper, J. T., Cheng, J., Pandya, U., Clark-Wronski, J., Awasthi, S., and Awasthi, Y. C. (1999) *Arch. Biochem. Biophys.* **367,** 216–224
20. Yang, Y., Cheng, J. Z., Singhal, S. S., Saini, M., Pandya, U., Awasthi, S., and Awasthi, Y. C. (2001) *J. Biol. Chem.* **276,** 19220–19230
21. Board, P. G. (1998) *Biochem. J.* **330,** 827–831
22. Bruns, C. M., Hubatsch, I., Ridderstrom, M., Mannervik, B., and Tainer, J. A. (1999) *J. Mol. Biol.* **288,** 427–439
23. Hou, L., Honaker, M. T., Shireman, L. M., Balogh, L. M., Roberts, A. G., Ng, K. C., Nath, A., and Atkins, W. M. (2007) *J. Biol. Chem.* **282,** 23264–23274
24. Hubatsch, I., Ridderstrom, M., and Mannervik, B. (1998) *Biochem. J.* **330,** 175–179
25. Alary, J., Debrauwer, L., Fernandez, Y., Cravedi, J. P., Rao, D., and Bories, G. (1998) *Chem. Res. Toxicol.* **11,** 130–135
26. Alary, J., Gueraud, F., and Cravedi, J. P. (2003) *Mol. Aspects Med.* **24,** 177–187
27. Awasthi, Y. C., Ansari, G. A., and Awasthi, S. (2005) *Methods Enzymol.* **401,** 379–407
28. Boon, P. J., Marinho, H. S., Oosting, R., and Mulder, G. J. (1999) *Toxicol. Appl. Pharmacol.* **159,** 214–223
29. Alin, P., Danielson, U. H., and Mannervik, B. (1985) *FEBS Lett.* **179,** 267–270
30. Singhal, S. S., Zimniak, P., Awasthi, S., Piper, J. T., He, N. G., Teng, J. I.,

Petersen, D. R., and Awasthi, Y. C. (1994) *Arch. Biochem. Biophys.* **311,** 242–250
31. Hashimoto, M., Sibata, T., Wasada, H., Toyokuni, S., and Uchida, K. (2003) *J. Biol. Chem.* **278,** 5044–5051
32. Hiratsuka, A., Hirose, K., Saito, H., and Watabe, T. (2000) *Biochem. J.* **349,** 729–735
33. Hiratsuka, A., Tobita, K., Saito, H., Sakamoto, Y., Nakano, H., Ogura, K., Nishiyama, T., and Watabe, T. (2001) *Biochem. J.* **355,** 237–244
34. Brichac, J., Ho, K. K., Honzatko, A., Wang, R., Lu, X., Weiner, H., and Picklo, M. J., Sr. (2007) *Chem. Res. Toxicol.* **20,** 887–895
35. Gueraud, F., Crouzet, F., Alary, J., Rao, D., Debrauwer, L., Laurent, F., and Cravedi, J. P. (2005) *BioFactors* **24,** 97–104
36. Honzatko, A., Brichac, J., Murphy, T. C., Reberg, A., Kubatova, A., Smoliakova, I. P., and Picklo, M. J., Sr. (2005) *Free Radic. Biol. Med.* **39,** 913–924
37. Gill, S. C., and von Hippel, P. H. (1989) *Anal. Biochem.* **182,** 319–326
38. Lu, W. D., and Atkins, W. M. (2004) *Biochemistry* **43,** 12761–12769
39. Nadkarni, D. V., and Sayre, L. M. (1995) *Chem. Res. Toxicol.* **8,** 284–291
40. Sashidhar, R. B., Capoor, A. K., and Ramana, D. (1994) *J. Immunol. Methods* **167,** 121–127
41. Ji, B., Ito, K., Suzuki, H., Sugiyama, Y., and Horie, T. (2002) *Free Radic. Biol. Med.* **33,** 370–378
42. Brunger, A. T., Adams, P. D., Clore, G. M., DeLano, W. L., Gros, P., Grosse-Kunstleve, R. W., Jiang, J. S., Kuszewski, J., Nilges, M., Pannu, N. S., Read, R. J., Rice, L. M., Simonson, T., and Warren, G. L. (1998) *Acta Crystallogr. Sect. D Biol. Crystallogr.* **54,** 905–921
43. Nilsson, L. O., Gustafsson, A., and Mannervik, B. (2000) *Proc. Natl. Acad. Sci. U. S. A.* **97,** 9408–9412
44. Aldini, G., Carini, M., Beretta, G., Bradamante, S., and Facino, R. M. (2002) *Biochem. Biophys. Res. Commun.* **298,** 699–706
45. Beretta, G., Artali, R., Regazzoni, L., Panigati, M., and Facino, R. M. (2007) *Chem. Res. Toxicol.* **20,** 1309–1314
46. Cameron, A. D., Sinning, I., L'Hermite, G., Olin, B., Board, P. G., Mannervik, B., and Jones, T. A. (1995) *Structure* **3,** 717–727
47. Reinemer, P., Dirr, H. W., Ladenstein, R., Huber, R., Lo Bello, M., Federici, G., and Parker, M. W. (1992) *J. Mol. Biol.* **227,** 214–226
48. Sinning, I., Kleywegt, G. J., Cowan, S. W., Reinemer, P., Dirr, H. W., Huber, R., Gilliland, G. L., Armstrong, R. N., Ji, X., Board, P. G., Olin, B., Mannervik, B., and Jones, T. A. (1993) *J. Mol. Biol.* **232,** 192–212
49. Ramana, K. V., Bhatnagar, A., Srivastava, S., Yadav, U. C., Awasthi, S., Awasthi, Y. C., and Srivastava, S. K. (2006) *J. Biol. Chem.* **281,** 17652–17660
50. Sharma, R., Sharma, A., Yang, Y., Awasthi, S., Singhal, S. S., Zimniak, P., and Awasthi, Y. C. (2002) *Acta Biochim. Pol.* **49,** 693–701